Geophys. J. Int. (1994) **118,** 142–158

Modified frequency-wavenumber algorithm for regional seismograms using Filon's quadrature: modelling of L_g waves in eastern North America

Chandan K. Saikia
Woodward–Clyde Consultants, 566 El Dorado St, Pasadena, CA 91101, USA

Accepted 1994 January 11. Received 1993 May 18; in original form 1993 January 21

SUMMARY

The main focus of this study is to develop an efficient frequency-wavenumber code to synthesize high-frequency (say, 10 Hz) regional seismograms (up to a distance of more than 1000 km) in a medium consisting of a large number of crustal layers, and investigate effects of regional waveguides on L_g waves. In this newly developed code, the frequency-wavenumber response is evaluated by using the Filon's quadrature at high frequency and the polynomial approximation of Bessel's functions (implementing trapezoidal integration) at low frequency. This has reduced the computation time by several folds compared to the time needed for the trapezoidal integration. Using this algorithm, both broad-band seismograms at Harvard and short-period ECTN (Eastern Canadian Telemetered Network) seismograms from 1988 November 25 Saguenay earthquake were successfully modelled. A moment magnitude of 5.9 was used. Initially an average waveguide was calibrated to successfully excite the regional P_{nl} and S_{nl} waves at HRV, its near-surface structure constrained by matching the recorded frequency content. The crust–mantle transition zone was constrained by modelling the strength of the broad-band S_{nl} waves, consisting of S_n, sS_mS_n, S_mSS_mS, and sS_mSS_mS phases, relative to the initial P_{nl} waves. The model was modified to consist of thin layers with an alternating high- and low-velocity distribution to match the high-frequency ECTN L_g waves observed from 300 to 600 km away. In addition, the effect of a near-surface irregular receiver structure on the duration of L_g waves was also investigated by convolving its response with the regional L_g seismograms. Initial study suggests this method as viable for modelling the entire L_g waves including the coda. Numerical studies suggest that the shapes and peak amplitudes on L_g seismograms depend more strongly on the source depth, anelasticity and crustal waveguide than do the P_{nl} seismograms.

Key words: Filon's quadrature, frequency wavenumber, irregular receiver crust, L_g waves, laminar structure.

1 INTRODUCTION

Recent investigations of high-quality regional seismograms recorded digitally have increased significantly our understanding of the high-frequency characteristics as influenced by crustal structure and source process. Many distinct features observed on the broad-band seismograms have been modelled in several studies for regional wave-propagation models (Dreger & Helmberger 1991; Vogfjord & Langston 1991; Zhao & Helmberger 1991; Saikia & Helmberger 1994; Saikia, Helmberger & Burdick 1992). The major task in modelling regional seismograms is the understanding of the complexity caused by wave propagation, especially in the composition of short-period waves. In a recent study, Saikia & Burdick (1991) have shown that short-period regional features at periods as short as 2 s

recorded within the P_{nl} window can be deterministically modelled and their composition can be deciphered using ray theory. In this study, we present a similar deterministic approach to understand the composition of the high-frequency S_{nl} waves by developing crustal waveguides consistent with the amplitudes and traveltimes of identifiable regional phases, and explore the ways to explain causes affecting the composition of the L_g waves.

To simulate the high-frequency seismograms, we utilized the frequency-wavenumber integration method. In th original frequency-wavenumber (F-K) integration techniqu (Fuchs & Muller 1971; Bouchon 1981), the invers Fourier–Bessel transformation $\int_0^\infty F(\omega, k)J_n(kr)k\,dk$ (wher $F(\omega, k)$ is the F-K kernel, $J_n(kr)$ is the nth order Bess function and k is the horizontal wavenumber) is evaluate using the polynomial approximations of the Bessel' functions. This requires a small wavenumber sampling rat due to the oscillation of the integrand caused by the Bessel'

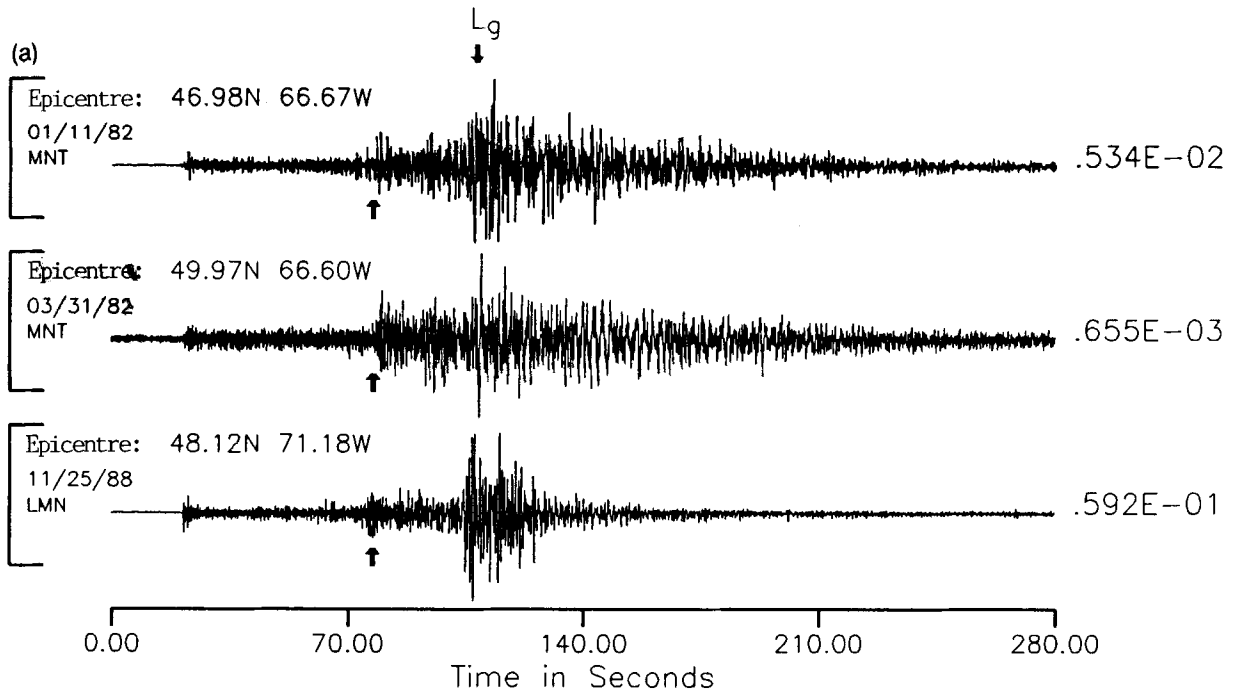

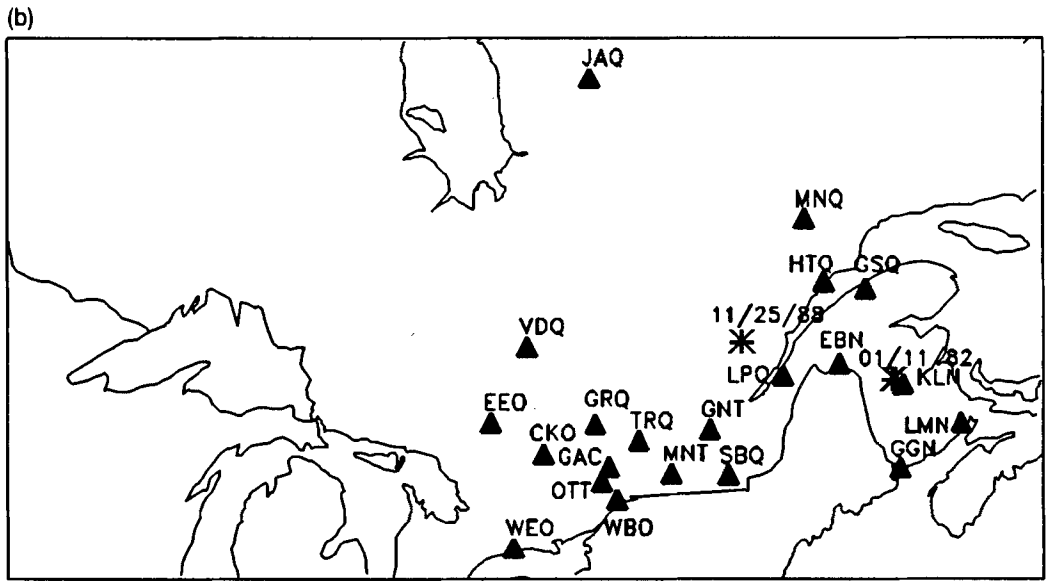

Figure 1. (a) Examples of regional L_g waves recorded from three North American earthquakes on the ECTN (Eastern Canadian Telemetere Network) stations. The arrows show the arrivals of P_n phases associated with S_n and L_g waves. (b) Map showing the geographical locations the ECTN stations (solid triangles) and the epicentres of the 1982 January 11 New Brunswick earthquake and the 1988 November 25 Saguena earthquake.

function. Therefore, we implemented a modified algorithm in which the transformation is evaluated using Filon's quadrature (Frazer 1977; Luco & Apsel 1983) at high frequency and Bouchon's integration criteria (Bouchon 1981) at low frequency.

Among the various phases, the most commonly observed seismic waves on seismograms of a local network are the L_g waves. Fig. 1(a) shows vertical component regional seismograms from three North American earthquakes recorded on the ECTN (Eastern Canadian Telemetered Network) stations, approximately at 540 km away from the epicentre. The upper two seismograms were recorded at Montreal (MNT) station for two separate earthquakes on 1982 January 11 and 1982 March 31; are the aftershocks of the 1982 New Brunswick earthquake. The lower seismogram was recorded at station LMN from the 1988 November 25 Saguenay earthquake in Quebec, Canada. Fig. 1(b) is a map showing the locations of the ECTN stations and these three earthquakes. Although the source mechanism and size of these earthquakes are different, the waveforms are characteristically similar, especially from the start of the S_{nl} waves (marked by the arrow) till the L_g waves, suggesting that the regional waveguides along these paths are probably similar.

The recent advent of theoretical methods to compute complete synthetic seismograms (Fuchs & Muller 1971; Kind 1979; Kennett 1980; Bouchon 1981) has greatly enhanced our understanding of the L_g wave excitation and their propagation characteristics. The investigations of Kim (1987), Campillo, Bouchon & Massinon (1984), and Olsen, Braile & Stewart (1983) can be cited as some of the examples. In a recent study, Campillo & Paul (1992) demonstrated that the L_g waves can be excited by the randomness of the lower crust, which they represented by a discretized crustal waveguide consisting of a laminar structure with an alternate high- and low-velocity variation. They found that this waveguide has a strong effect on the duration of both P_g and L_g waves. The regional seismograms recorded on the Eastern Canadian Telemetered Network (ECTN) also show strong L_g waves. To model these L_g waves, we have developed an initial waveguide by modelling the frequency content, amplitude and phase splitting observed on the broad-band seismograms recorded at Harvard station from the 1988 November 25 Saguenay earthquake. These seismograms were selected for two reasons. First, the source process of the Saguenay earthquake event has been previously studied (Somerville *et al.* 1990; Haddon 1992). Secondly, Zhao & Helmberger (1991) modelled many features recorded on these waveforms. The preferred crustal model was modified to include a random velocity fluctuation by comparing the predicted L_g waves with those recorded on the ECTN seismograms up to a distance of 616 km.

A model perturbation was also included in the receiver crust to excite the later part of the L_g waves, also known as the coda waves. The real earth structure is not flat and the receiver crust is possibly non-uniform. The origin of L_g coda may be related to the random scatterers present within a receiver structure (Aki & Chouet 1975; Frankel & Clayton 1984; Wu 1985) or non-uniform receiver structures (Barker, Der & Mrazek 1981; Bard *et al.* 1988; Campillo *et al.* 1988; Kawase & Aki 1989). Based on the single-scattering approximation theory, proposed by Tolstoy & Clay (1966), Aki & Chouet (1975) treated L_g coda as the backscattered seismic waves from the random scatterers based on the single-scattering approximation theory, proposed by Tolstoy & Clay (1966). In case of a first-order multiple-scattering problem and increased particle density, the scattered wavefield from one particle is further scattered by another particle complicating the wavefield even more.

There may also exist discontinuous low-velocity geological materials pinching out at the surface which may provide additional waveguides for these late waves. In a recent study, Saikia, Dreger & Helmberger (1994) have demonstrated that if the regional waves arrive at the base of a non-uniform structure at shallow angles, the pockets of discontinuous low-velocity surface materials act as delay operators increasing the signal duration. Thus, a physical mechanism may be proposed for generating L_g waves which is perhaps a combination of a laminated structure for the lower crust and non-uniform structure near the receiver. Another type of wavefield scattering is caused by perturbing velocities in the propagation medium (Aki & Richards 1980). In addition to the scattering effect (Q_s) introduced by the heterogeneous crustal structure, the attenuation of elastic waves due to the intrinsic Q_I is the other primary means for the loss of seismic energy. Some results are also presented demonstrating the possible effects of Q_s and Q_I on the various regional phases.

2 FREQUENCY-WAVENUMBER ALGORITHM

The essence of the present frequency-wavenumber algorithm is to propagate the stress-displacement vector through a heterogeneous crustal medium consisting of many horizontally stratified isotropic layers, and its numerical scheme has been discussed in several papers (Haskell 1964; Dunkin 1965; Wang & Herrmann 1980; Herrmann & Wang 1985). To summarize briefly, Haskell (1964) formulated the original method for propagating the wavefield from an embedded source using a propagator-matrix method which involves multiplications of many 4×4 layer matrices. But it had a serious drawback in that the elements of the layer matrices had exponentially growing terms involving $\exp(\pm\nu_\alpha z)$ and $\exp(\pm\nu_\beta z)$ where α and β are the compressional and shear velocities respectively, and $\nu_\alpha = \sqrt{k^2 - k_\alpha^2}$ and $\nu_\beta = \sqrt{k^2 - k_\beta^2}$, k are horizontal wavenumbers. These terms grow with increasing z (layer thickness) and frequency. The exponentially growing terms can, however, be analytically cancelled using a compound matrix formulation (Dunkin 1965; Watson 1970) which is also applied in the present algorithm.

In the frequency-wavenumber/reflectivity method, an integral given by

$$F(\omega, r) = \int_0^\infty F(k, \omega) k J_n(kr)\, dk \qquad (1)$$

(where $F(k, \omega)$ is the medium response (see the Appendix for details), $J_n(kr)$ is the nth order Bessel's function and k is the horizontal wavenumber) is evaluated. The above integral can be evaluated using the criteria presented in Bouchon (1981) in which the Bessel functions are

represented by their polynomial approximations (Abramowitz & Stegun 1970). These polynomials are truncated with errors in the order of 10^{-8}. Both for the earthquakes and the explosions, the Bessel's functions are required up to the second order, for most cases r appearing in the denominator (Herrmann & Wang 1985). As r approaches zero, additional higher-order terms involving r^{-n} become important, especially at long periods. In addition, the integrand is also highly oscillatory with increasing frequency and distance. Consequently, a fine sampling of the wavenumber axis is needed to avoid any spatial aliasing. This leads to a large computation time for the synthesis of a regional seismogram. The size of the wavenumber interval Δk (where $\Delta k = 2\pi/L$) is decided through the criteria given by

$$L > 2r$$

and

$$\sqrt{(l-r)^2 + h^2} > v_{\max} T, \tag{2}$$

where $v_{\max}$, h and T are the highest velocity, the depth of the seismic source and the length of the time series, respectively. These two criteria are adequate in most cases for sampling the wavenumber axis.

The Filon's quadrature interpolation scheme, an alternative to the above integration scheme, has proved superior in reducing the needed computation time (Frazer 1977; Frazer & Gettrust 1984). This interpolation scheme has been successfully implemented to synthesize reflectivity seismograms (Mallick & Frazer 1988). To apply the Filon's quadrature interpolation scheme, the Bessel's functions are approximated in terms of equivalent Hankel functions which include only the outgoing wavefield. With this approximation and retaining only the far-field terms, eq. (1) reduces to

$$F_n(\omega, r) = \sqrt{\frac{2}{\pi kr}} \int_0^\infty F(k, \omega) k \exp\left[-i(kr - n\pi/2 - \pi/4)\right] dk$$

$$= \sqrt{\frac{2}{\pi r}} \int_0^\infty \bar{F}(\omega, k) \exp(-ikr)\, dk. \tag{3}$$

The above expression is of the form $\int_0^\infty \bar{F} \exp[\sigma g(k)]\, dk$ (Frazer 1977) where $\sigma = -ir$ and $g(k) = k$. For a piecewise continuation of $\bar{F}(k)$ and $g(k)$ given by

$$\bar{F}(k) = \bar{F}_{j-1} + \frac{\bar{F}_j - \bar{F}_{j-1}}{\Delta} k$$

$$g(k) = g_{j-1} + \frac{g_j - g_{j-1}}{\Delta} k, \tag{4}$$

we can evaluate the integral (3) between two arbitrary limits of k_1 and k_2 by parts and write

$$\int_{k_1}^{k_2} \bar{F}(\omega, k) \exp(-ikr)\, dk$$

$$= -\frac{1}{ir}\left[\left[\bar{F}(k_2)\exp(-ik_2 r) - \bar{F}(k_1)\exp(-ik_1 r)\right] - \frac{\left[\bar{F}(k_2) - \bar{F}(k_1)\right]\left[\exp(-ik_2 r) - \exp(-ik_1 r)\right]}{ir(k_2 - k_1)}\right]. \tag{5}$$

Evaluating the integral (1) using the above quadrature is economical because the kernel $\bar{F}$ oscillates slowly and the function $g(k)$ is a monotonically increasing function of k. Thus, a larger interval dk is permitted for sampling the real k-axis. On the other hand, the integrand $\bar{F}(\omega, k)\exp(-ikr)$ is a highly oscillatory function for which an integration by using the trapezoidal interpolation scheme would require a finer sampling interval. This is demonstrated in Fig. 2 where the real and imaginary parts of the kernel $\bar{F}(\omega, k)$ are shown for two frequencies, 1 and 5 Hz, respectively, at distances of 75 and 300 km. The results for 1 Hz are shown in Fig. 2(a). The real and imaginary parts of the function $\bar{F}(\omega, k)\exp(-ikr)$ are also shown. While the real and imaginary parts of $F(\omega, k)$ are relatively smooth, the real and imaginary parts of the integrand $F(\omega, k)\exp(-ikr)$ are oscillatory, the oscillation being large at 300 km. The results are the same for 5 Hz (Fig. 2b) where the oscillation of the integrand $F(\omega, k)\exp(-ikr)$ has increased sharply. However, the $F(\omega, k)$ kernel is still smoothly varying, permitting a large step size in wavenumber for interpolating the function and for evaluating the integral (3) using Filon's quadrature without introducing a significant error. The kernel is more oscillatory at 5 Hz. So a smaller dk interval must be used compared to the dk interval chosen at 1 Hz.

In this newly developed code, we use a trapezoidal integration scheme, implementing the Bouchon's criteria given by eq. (2), to evaluate the response at a low frequency and the Filon's quadrature scheme at a high frequency. The switch from one integration scheme to the other is automatic in the code using the following strategy. First, the number of points needed to sample the wavenumber axis using the criteria presented in eq. (2) is determined using an upper limit $k_{\max}$ for the integration where $k_{\max}$ is a user-specified value so that the contributions from the required ray parameters are included in the integrand. The number of wavenumber points is also determined for the Filon's quadrature method using a slightly smaller step size as presented in Frazer & Gettrust (1984). The method with the smaller wavenumber points is used to compute the response of the medium.

The results shown in Fig. 2 were computed using a crustal model consisting of a 40 km thick layer with a P-wave velocity of 6.15 km s^{-1} and an S-wave velocity of 3.5 km s^{-1} over a half-space with P and S velocities of 8.09 and 4.67 km s^{-1}, respectively. The densities of the two layers were 2.8 and 3.3 gm cm^{-3}, respectively. Fig. 3 compares Green's functions computed for eight fundamental faults and an explosion source using the two integration methods. The Nyquist is 10 Hz and the distance is 75 km. The two sets of Green's functions are remarkably similar except for the peak amplitudes.

3 MODELLING REGIONAL SEISMOGRAMS

Here we analyse the effect of the regional waveguide on various regional phases including the L_g waves. We selected seismograms from an earthquake whose source process has been reliably established. As pointed out earlier, the 1988 November 25 Saguenay earthquake is an example of one such moderate-sized North American earthquake. First, we refine the Zhao & Helmberger model to improve the fit between the data and synthetics using the same Harvard broad-band seismograms. Second, we demonstrate how the site response affects both the amplitude and duration of the L_g waves, including the high-frequency L_g coda wave

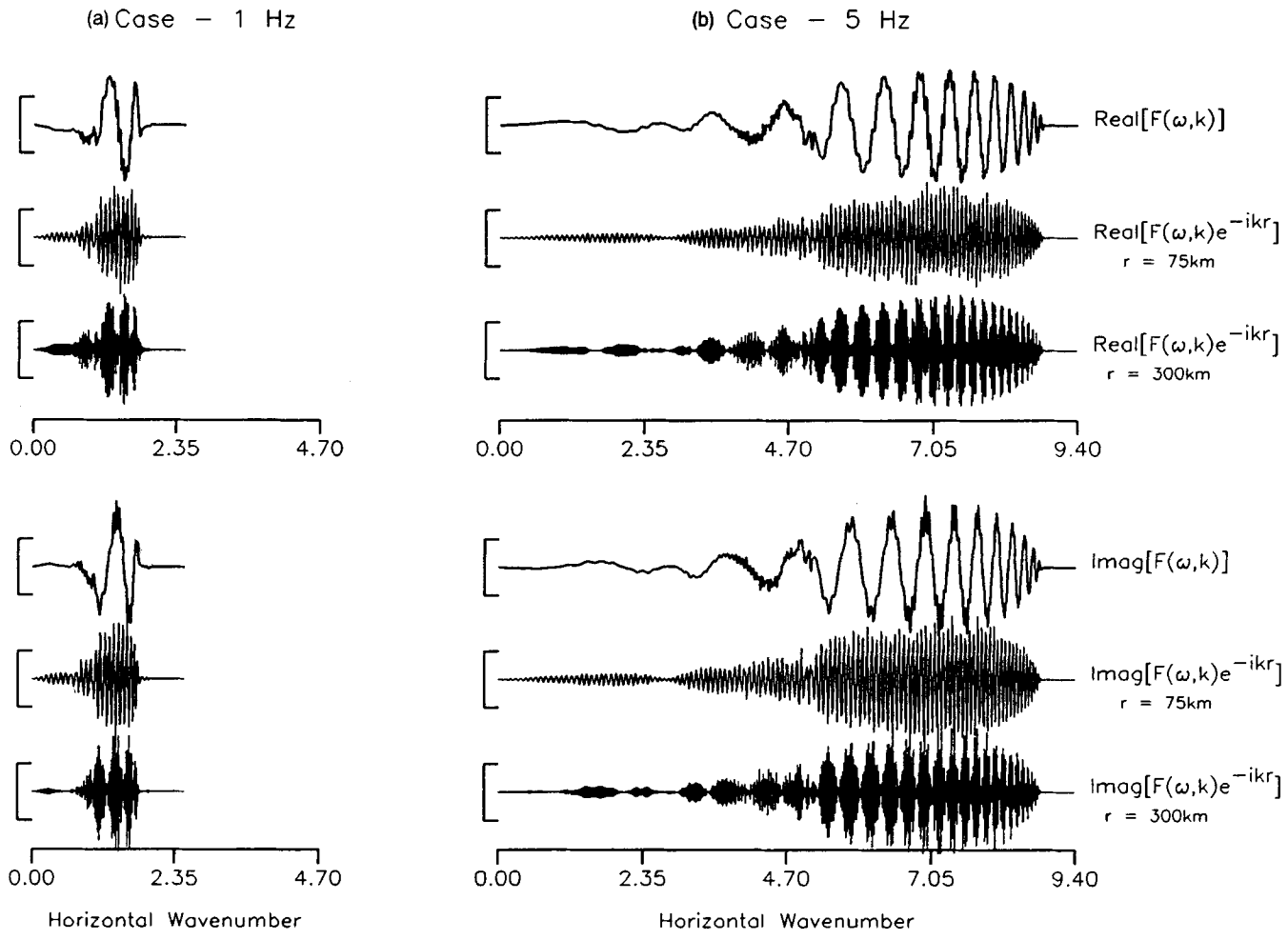

Figure 2. The real and imaginary parts of the kernel $F(k, \omega)$ and integrand $[F(k, \omega) \exp(-ikr)]$ at distances, 75 and 300 km, respectively, for 1 and 5 Hz signals; (a) for 1 Hz and (b) for 5 Hz. While both the real and imaginary parts of $F(k, \omega)$ kernel vary smoothly with k, the integrands oscillate significantly. The oscillation is large with distance and frequency.

duration. It has been suggested that the coda waves following the L_g waves are caused by random scatters (Aki 1969; Aki & Chouet 1975). Below we examine how random scatterers or irregular receiver crusts influence the coda waves.

3.1 Data

To date, the 1988 November 25 Saguenay earthquake, in Quebec, Canada is the largest eastern North American earthquake providing both strong and weak motion recordings. The strong motions are recorded from 42 km range to about 300 km. The weak motions are recorded on the short-period Eastern Canadian Telemetered Network (ECTN, Fig. 1) stations at distances from 300 to 700 km (North *et al.* 1989). In this study, we used seismograms from eight stations: SBQ, GRQ, KLN, WBO, GGN, CKO, LMN and EEO. The farthest station EEO is located at 616 km from the source. Stations located further away are not included to minimize the computation time.

3.2 Modelling of broad-band Harvard seismograms

Zhao & Helmberger (1991) presented synthetic seismograms showing a fair agreement with the broad-band seismograms recorded at Harvard station from the Saguenay earthquake. The synthetic seismograms were deficient in short-period energy following the onset of P waves until the arrival of Moho-reflected S waves. Also, the synthetics of the S_n and sS_n phases could be improved. The present study started with an aim to reduce these misfits and develop a new crustal model (MODEL 1, Fig. 4; see Table 1). The new model consists of a velocity gradient in the upper 5 km of the crust where the P-wave velocities were reduced from 6.6 km s^{-1} to 6.1 km s^{-1} and the S-wave velocity from 4.5 km s^{-1} to 3.5 km s^{-1} at the surface. The gradient structure in the upper crust changes the frequency of the recorded seismograms at the receiver because the free-surface reflection coefficients and the timing of the waves change due to the gradient. Additionally, added reverberations of seismic waves start beneath the receiver

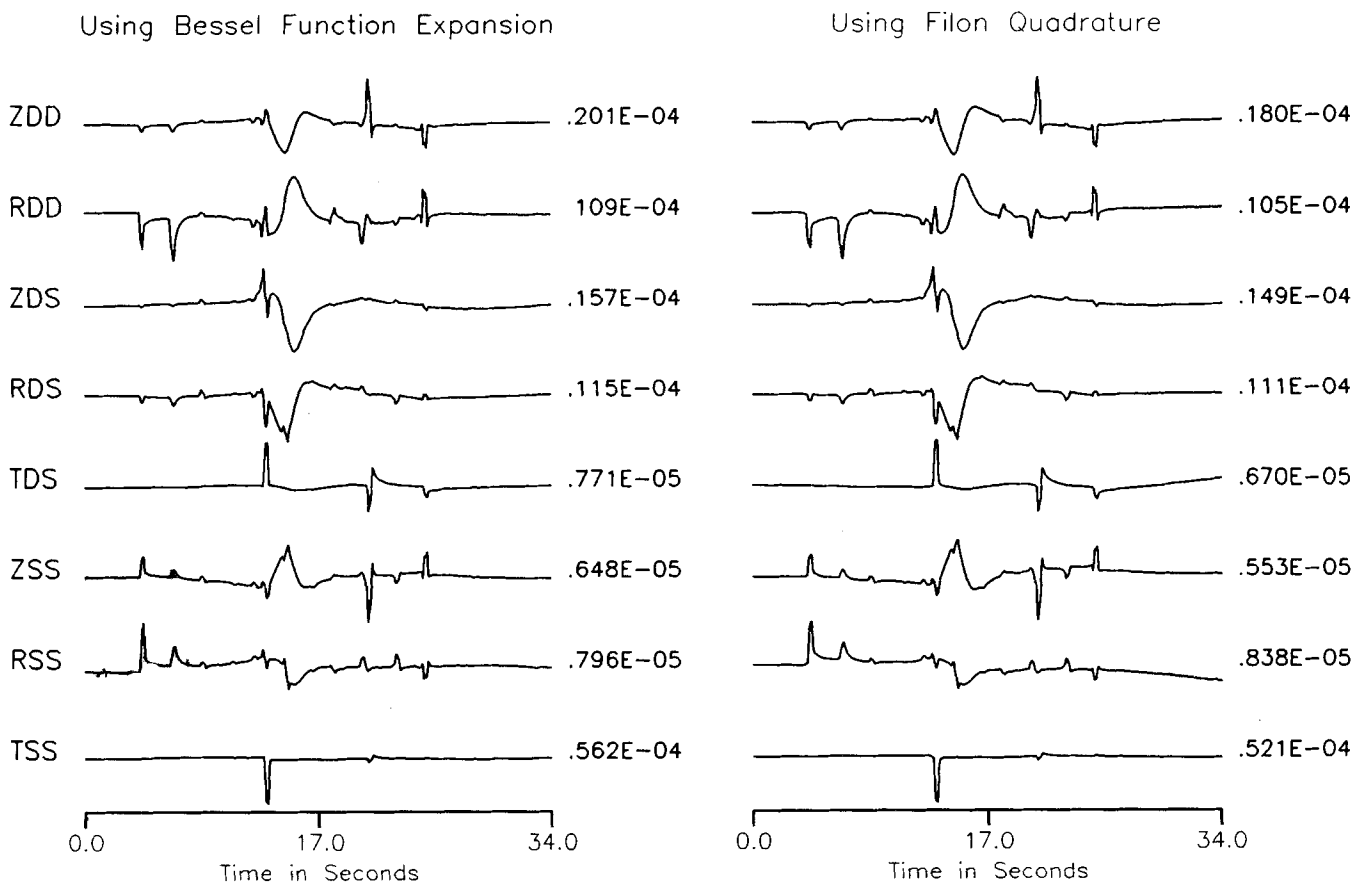

Figure 3. Comparison of Green's functions synthesized by evaluating the inverse Fourier–Bessel transformation (1) using the trapezoidal integration scheme with full expansion of Bessel functions and the Filon's quadrature scheme using only the asymptotic term of the Bessel's functions.

structure. The model consists of another small gradient for the S waves across the crust–mantle transition zone in the upper mantle region which forces the classical head waves to turn and arrive with strong amplitudes.

Figure 5(a) displays the synthetic seismograms plotted beneath the recorded seismograms. The traveltimes of the Rayleigh waves have a slight mismatch. The initial parts of the P_{nl} and S_{nl} waves are shown separately in Fig. 5(b). The agreement between the data and the synthetics is remarkably good, especially the relative amplitude and frequency content of the P_{nl} to the S_{nl} waves. The complexity in three phases (each marked by an arrow) on the vertical component is caused by the multiple-source effect and is predicted reasonably well. The source function of the first source was represented by a trapezoid of 0.4 s rise time, 0.05 s of follow-on time and 0.25 s of healing time. A seismic moment of 1.55×10^{24} dyne-cm was used. Similarly, the second source was represented by a trapezoid of 0.2 s rise time, 0.15 s follow-on-time, and 0.15 s of healing time with a seismic moment of 1.45×10^{24} dyne-cm, and the third source by a trapezoid of 0.1 s rise time, 0.3 s of follow-on time, and 0.2 s of healing time with a seismic moment of 1.95×10^{24} dyne-cm, respectively. The contributions of individual sources were added together with delay times represented by a rupture velocity of 2.5 km s^{-1}.

Figure 6 shows a decomposition of the constituent phases recorded in the P_{nl} waves in the above seismograms. We synthesized ray seismograms for six groups of generalized rays using the multiple-source process discussed above. The amplitudes of the upper six seismograms are normalized by their peak amplitude. The P_mP and S_mS rays were allowed to reflect from each interface beneath the crust–mantle boundary including the reflection from the Moho discontinuity. The total response of these phases is plotted in the first seismogram. The geometric arrival of S_mS ray is shown. The S_n arrival is small and is preceded by a refracted phase S_nP. This refracted phase has developed due to critical incidence of an S wave at the free surface permitting the converted P phase to travel along the interface. The seismogram in the second row is for sP_mP, a ray which departed upward from the source as an S wave and converted to P at the free surface. The amplitude of this ray group is small. The next seismogram is for sS_mS. Both the geometric and the head waves are strong for this ray group and contribute significantly to the total seismogram. The next two seismograms are for the S_mSS_mS and sS_mSS_mS ray groups, each having a significant contribution. The sixth seismogram is for a ray group identified as $S_mS^{(i)}S_mS$. The rays included in this group leave the source downward and are reflected from each interface. The reflections are turned

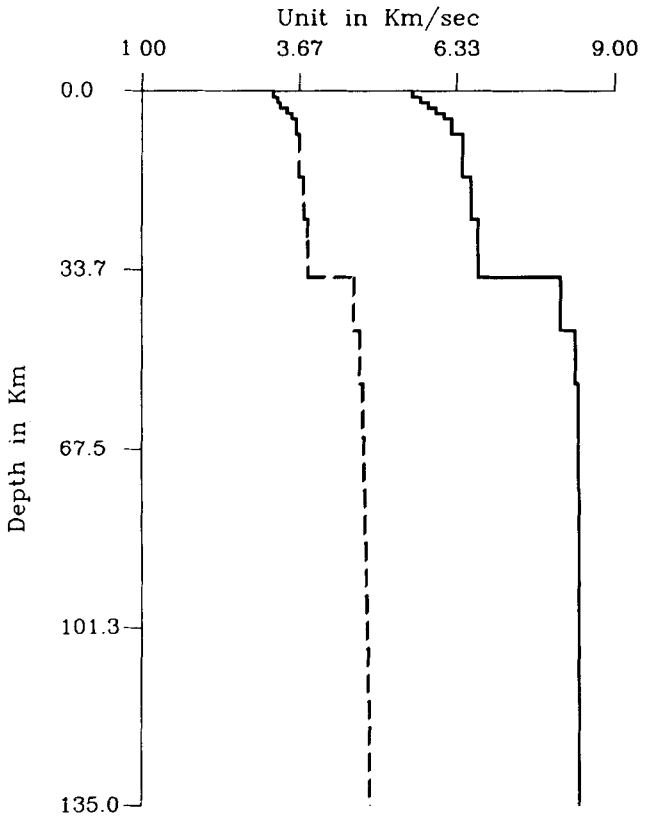

Figure 4. Regional crustal velocity model (MODEL 1) developed using the broad-band seismograms recorded at Harvard station from the 1988 November 25 Saguenay earthquake. This structure (Table 1) consists of a velocity gradient near the surface and across the crust–mantle transition zone.

Table 1. Average crustal model (MODEL 1) obtained by modelling Harvard seismograms.

P Velocity km/s	S Velocity km/s	Density gm/cm^3	Thickness km	Q_β
5.6	3.24	2.82	1.0	250
5.732	3.31	2.846	1.0	250
5.864	3.35	2.873	1.0	250
5.996	3.47	2.899	1.0	250
6.128	3.55	2.926	1.0	250
6.26	3.62	2.952	3.0	250
6.45	3.67	2.99	8.0	500
6.59	3.75	3.02	8.0	500
6.71	3.82	3.04	4.0	6200
6.71	3.82	3.04	7.0	6200
8.1	4.6	3.32	10.0	6200
8.35	4.7	3.37	10.0	6200
8.4	4.755	3.38	10.0	6200
8.41	4.775	3.387	10.0	6200
8.42	4.794	3.393	10.0	6200
8.421	4.813	3.4	10.0	6200
8.422	4.833	3.407	10.0	6200
8.425	4.852	3.413	10.0	6200
8.43	4.871	3.42		6200

back into the lower medium again at the Moho discontinuity before they are reflected back to the receiver. The contributions from these rays make a significant contribution to the evolution of the S_{nl} seismogram. The seismogram 'Total' is the direct sum of the upper sixth seismograms. The F-K seismogram is the final seismogram computed using the modified frequency-wavenumber algorithm and the same multiple-source description. The agreement between the last two seismograms suggests that the dominant features of the seismograms are identified and modelled.

Using the crustal model shown in Fig. 4 and the above multiple-source process, we synthesized high-frequency regional L_g waves at the ECTN stations. The comparison between the observed ECTN and the simulated L_g seismograms is shown in Fig. 7. For each synthetic seismogram, a small window of the P_{nl} seismogram is also displayed. A model dependence of this P_{nl} seismogram will be discussed in the next section. The ECTN seismograms were corrected to a common instrument response (Type III) which was also added to the synthetic seismograms. The agreement is obviously poor in both peak amplitudes and waveshapes, suggesting that the crustal model is not efficient in trapping high-frequency L_g waves. In the next section, we shall demonstrate that a crustal model consisting of thin layers with an alternating high- and low-velocity distribution is needed to trap these regional L_g waves.

3.3 Calibration of regional waveguide for L_g waves

Recently, it has been demonstrated that the regional L_g waves can be successfully generated (Campillo & Paul 1992). The method uses a laminated flat-layered waveguide with an alternating high- and low-velocity distribution across the entire crust. In fact, the concept of the laminar structure was initially introduced by Richards & Menke (1983) and O'Doherty & Anstey (1971) to investigate Q_s (scattering Q) at a local distance. Another recent study by Mallick & Frazer (1990) uses the same concept. Based on the same idea, we constructed several structure models consisting of many thin layers, allowing a random fluctuation of velocities within each layer, so that each random structure approximately represents the same average structure as presented in Fig. 4. For each velocity structure, the synthetic seismograms were simulated and compared with the data. If the agreement was poor, a new crustal model was sought. The quality of agreement was judged based on the following constraints: the relative amplitude of L_g waves compared to the amplitude of P_{nl} waves, the start time of the S_{nl} waves shown by arrows in Fig. 7, the relative traveltimes of various phases, and the waveform characteristics between the S_{nl} and L_g waves.

Figure 8 displays the final crustal structure (MODEL 2; see Table 2) which has a significant randomness within the crust and produced a reasonable agreement between data and synthetic L_g-wave seismograms (Fig. 9). The agreement is good up to the arrival of the early L_g waves. Also, the onset of the S_{nl} waves relative to the L_g waves is consistent with the observed onset. Except for station SBQ, the peak amplitudes are also predicted within a factor of two. The most remarkable agreement is observed at GGN. The data show extended duration, especially in the coda waves at some stations, which is perhaps related to the structure

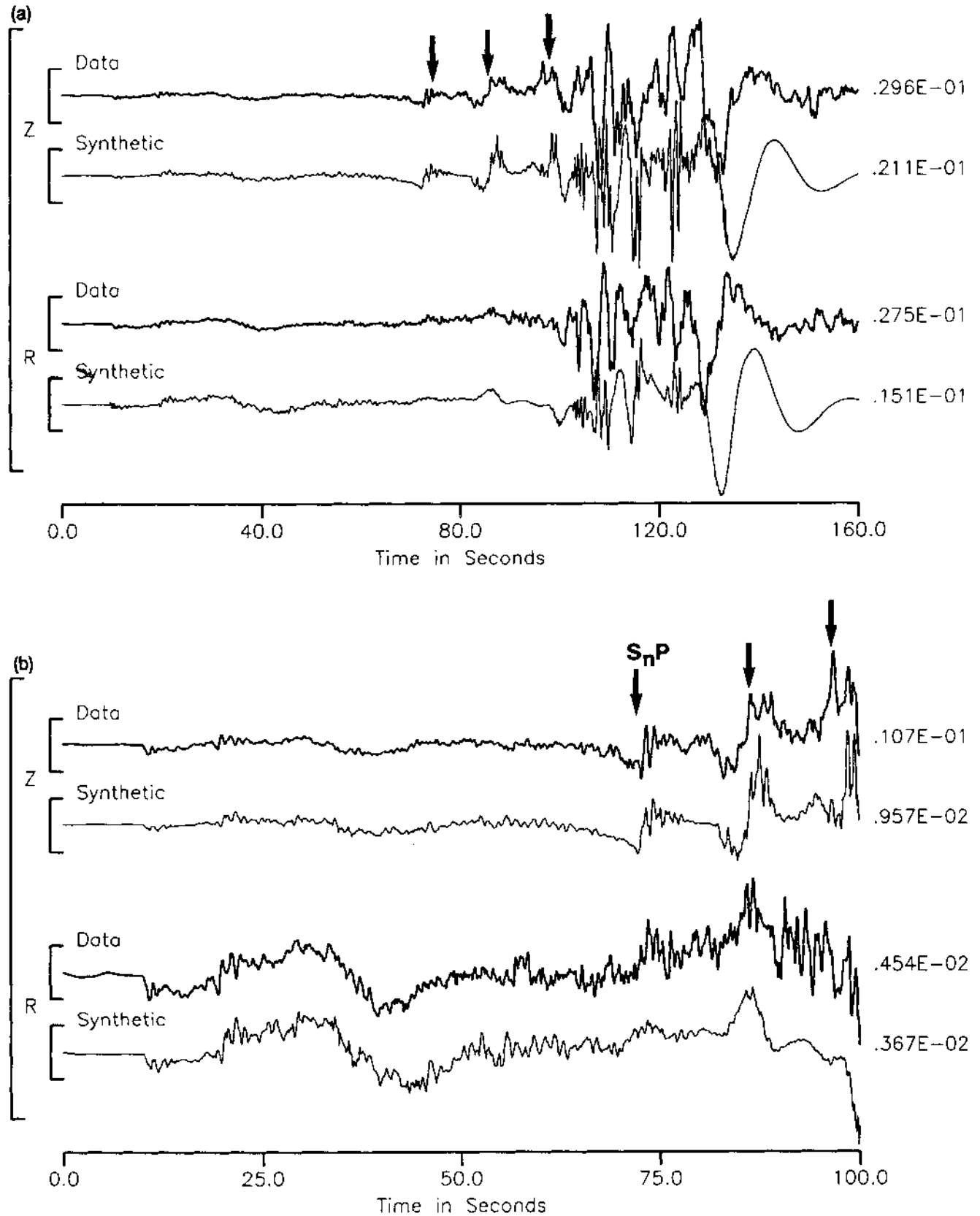

Figure 5. Comparison of data recorded at Harvard station from the 1988 November 25 Saguenay earthquake and synthetic seismograms computed using the crustal model shown in Fig. 4 and the source model discussed in the text. The comparison is for (a) the entire seismogram and (b) the first 100 s of the P_{nl} and the S_{nl} waves. Arrows indicate specific S_{nl} phases.

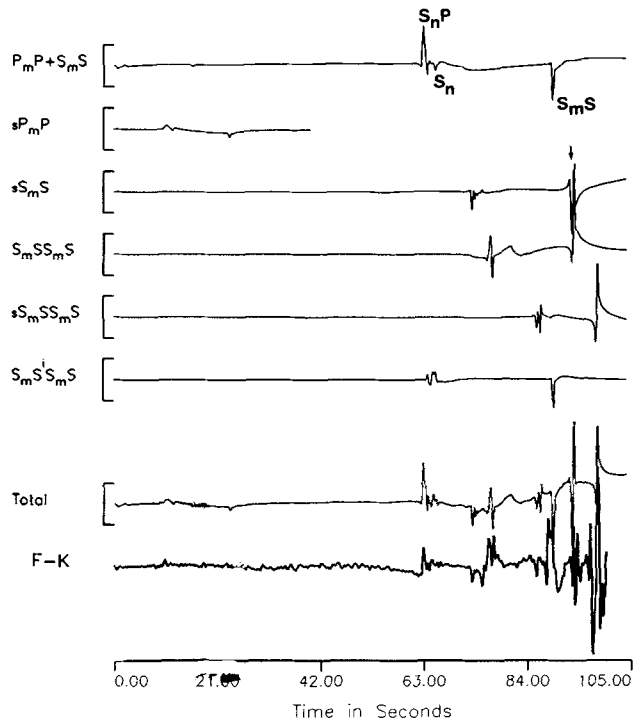

Figure 6. The ray composition of the P_n and S_{nl} waves. The seismograms 'TOTAL' is computed by adding the six seismograms shown for various ray groups. The seismogram 'F-K' is synthesized using the frequency-wavenumber integration algorithm. The close resemblance of these two seismograms suggests that the P_{nl} and S_{nl} seismograms can be synthesized by using just a limited number of ray groups even at large regional distance.

around the receiver crust. The distinct phases within the P_{nl} seismograms presented in Fig. 9 exhibit major similarities with those presented in Fig. 7. Thus it is quite convincing that the heterogeneity of the lower crust is mostly responsible for the L_g waves.

The ray interpretation presented earlier for the broad-band seismograms of Harvard station is found valid for the P_{nl} and S_{nl} waves recorded by the ECTN instrument. Fig. 10(a) shows the ray response of the same six groups of generalized rays at GGN based on the regional waveguide presented in Fig. 8. The synthetic seismogram 'Total' is constructed by adding the synthetics above it. The bottom seismogram is the actual ECTN short-period data recorded at GGN. To make a direct comparison with the ECTN data, the 'Total' response is convolved with a ECTN instrument and the resulting synthetic ECTN-SYNTH' is plotted above the data. There is a high correlation between the last two seismograms. Clearly, the waves that contribute most to the S_{nl} waves are the sS_mSS_mS waves. A comparison is presented in Fig. 10(b) for the complete seismograms which, in addition to the waveform characteristics, shows a remarkable agreement in the peak amplitude.

It was pointed out by North *et al.* (1989) that the m_{bLg} for the Saguenay earthquake obtained using regional seismograms ranging from 310 to 715 km is consistent, ranging from 6.4 to 6.7. This is a large value compared to the teleseismic magnitude m_b 5.9 (USGS National Earthquake Information Service). According to their study, other earthquakes of eastern Canada—including the New Brunswick earthquake of 1982, Cornwall earthquake of 1944, Charlevoix earthquakes of 1925 and 1939, and the Timiskaming earthquake of 1935—do not exhibit this discrepancy in the magnitude. Recently, Boore & Atkinson (1992) suggested that the Charlevoix event of 1925 may also be an 'anomalous' event. Interestingly, both the Saguenay and the New Brunswick earthquakes have the same m_b but very different m_{bLg}. They argued that this discrepancy is not related to propagation effects and that m_b is not a good indicator of L_g wave amplitude. Contrary to their findings, the peak amplitude of the L_g waves, simulated using a moment magnitude of 5.9, is consistent with the recorded peak amplitude.

3.4 L_g waves as affected by irregular receiver crust and embedded scatterers

Previous studies by Kawase & Aki (1989), Barker, Der & Mrazek (1981), Campillo *et al.* (1988) and others show that interaction of incident *SH*, *SV*, *P*, L_g or long-peiod Rayleigh waves with 2-D structure can significantly lengthen the duration of seismic wavefield. In a recent study, Saikia *et al.* (1994) have numerically shown that such interaction will elongate the duration of high-frequency regional waves. In this study, we demonstrate that the L_g coda waves can indeed be trapped by letting regional L_g waves interact with a localized irregular receiver structure, including the effects that may be produced by random scatterers embedded in a medium.

To examine the irregular receiver effect, we represent the regional L_g wavefield by the synthetic seismogram at WBO and use a simplified 2-D structure as shown in Fig. 11(a) with five receivers numbered 1 through 5 (shown by solid triangles). This irregular structure is not a representation of any physical structure for the ECTN stations but is used to understand the duration of L_g waves. Fig. 11(b) shows 12 s of the vertical component *P–SV* Green's functions at the receivers computed by permitting only the *S* waves to impinge on the structure at an angle of 11°. The complexity in the waveforms increases from site 1 to site 5 as caused by the waves trapped within the irregular part of the basin. The low-velocity material included at the surface increases the amplitude. The final seismograms shown on the right are obtained by convolving the regional L_g seismogram with each seismogram shown on the left. The overall change in duration is small because the duration of the corresponding seismogram on the left is also small. The changes in the frequency content and the sustained level of L_g waves relative to the frequency-wavenumber seismogram at WBO are distinctly noticeable at different receiver positions. If an irregular basement structure is added, the energy which is leaked into the half-space in the present model will be trapped, increasing the duration even more depending on the angle at which the regional wavefield impinges the local structure. Thus, the complexity exhibited in Fig. 11 will perhaps be more complex if the regional wavefields were to interact with the local structure at all angles simultaneously.

The strategic approach adopted in the above study is appropriately a hybrid of two numerical methods in which the frequency-wavenumber seismogram is convolved with

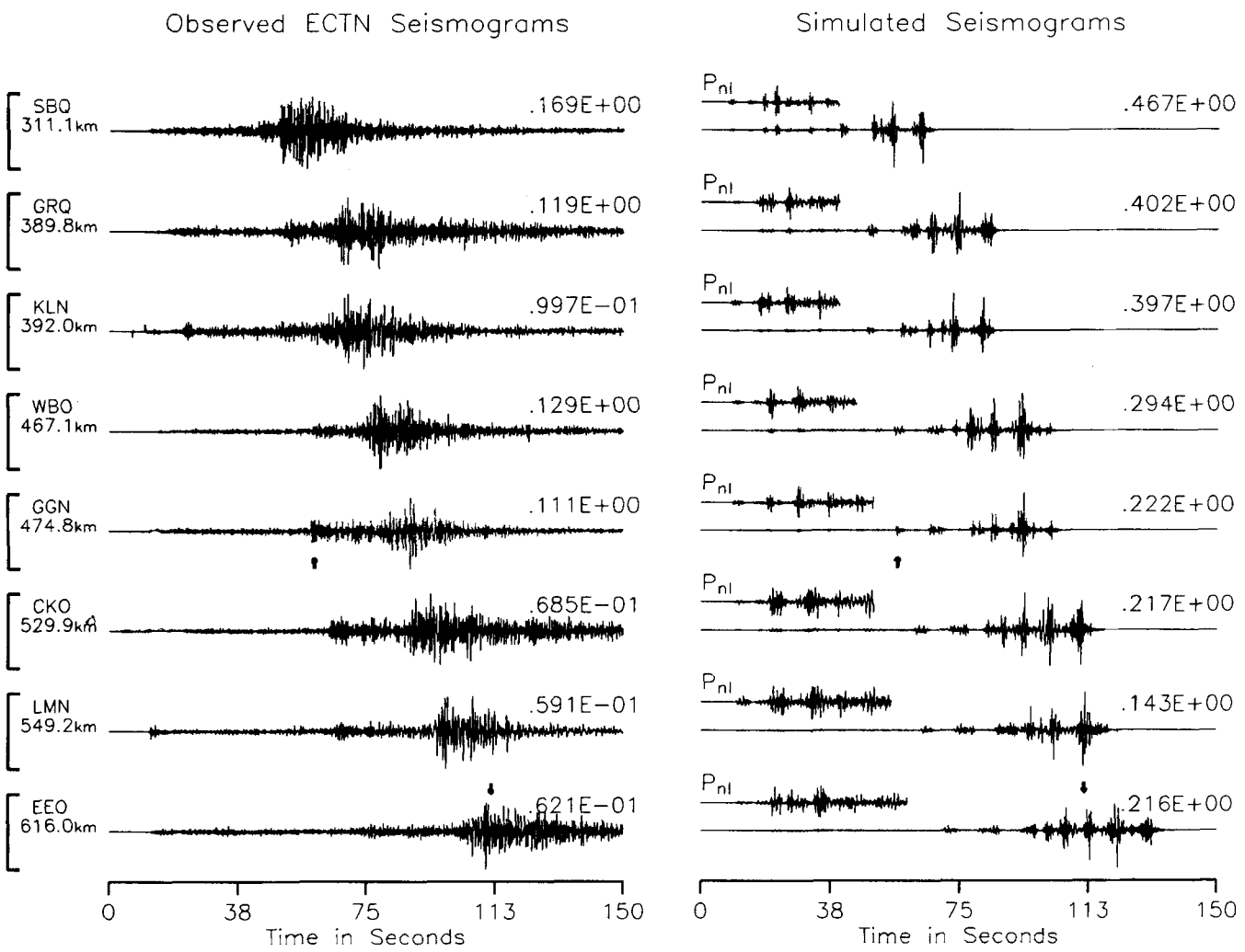

Figure 7. Comparison of the recorded ECTN seismograms with the synthetic seismograms computed using the structure MODEL 1 The agreement in the L_g waves is noticeably poor. The arrows show the agreement in the traveltimes of the S_n and S_nP waves.

the time-domain response of an irregular medium. A better method for an exact high-frequency seismogram is, however, to interface the frequency-wavenumber output directly with the finite-difference algorithm. This can be implemented by illuminating grid points located on the vertical and the bottom boundaries of the 2-D crustal structure with the regional wavefield and then allowing the wavefield to march through the model. However, this is beyond the scope of this study.

Embedded scatterers present within a crustal structure may also give rise to adequate excitation of regional L_g waves (Aki & Chouet 1975). A recent study has investigated the variation in the deterministically computed response up to 2 Hz as influenced by random scatterers within the layers f a crustal model (Helmberger *et al.* 1993). To explore ualitatively how the high-frequency L_g waves may be nfluenced by the presence of such a mechanism, we turn the RMOHO and RSURF response of Helmberger and co-workers (see Helmberger *et al.* 1993, for the variance and correlation lengths and other details of the models) at 10 stations into the ECTN seismograms. By examining the seismograms, we noted the following: the RSURF model produced seismograms where energy noticeably persisted for a longer duration, developed mostly by waves from the scatterers present within the surface layer. The low-velocity scatterers turn rays to different angles and sometimes act as delay operators. It was difficult to distinguish whether the mechanism of back or forward scattering was responsible for generating these coda waves as the scatterers were distributed everywhere within the entire layer, but the hypothesis that random scatterers would excite L_g waves is, nevertheless, promising.

4 EFFECT OF ATTENUATION ON REGIONAL SEISMOGRAMS: A NUMERICAL STUDY

So far, the results presented above are based on the elastic crustal models. In addition to the attenuation caused by scattering attenuation (Q_s) introduced by the velocity fluctuation, the intrinsic attenuation (Q_I) may also affect the regional L_g and P_{nl} waves. In this study, these effects are investigated using a moderate Q model since north-east America is a high Q province (Hasegawa 1983; Shin &

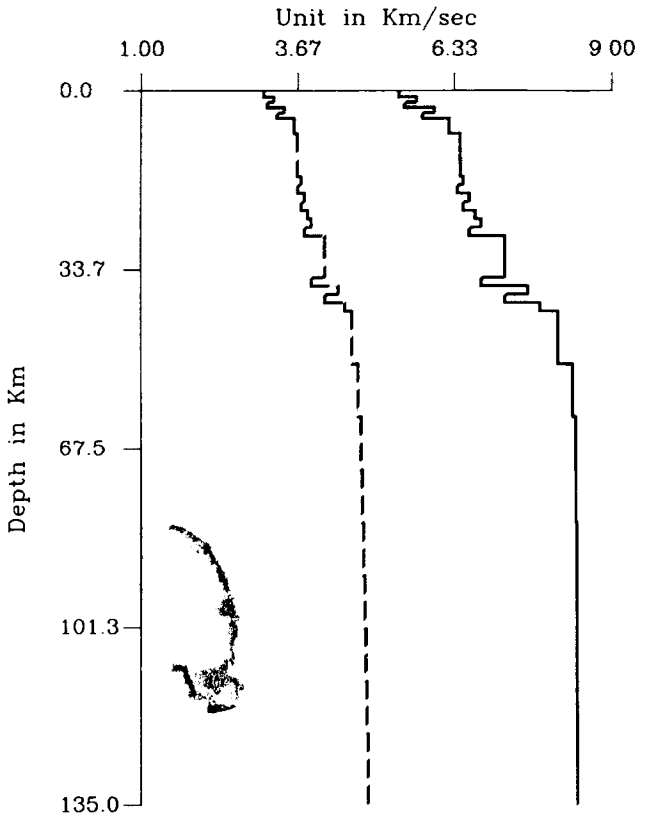

Figure 8. A crustal model (MODEL 2) appropriate for simulating the L_g waves developed using a canonical model search technique. This model (Table 2) consists of alternate high- and low-velocity distributions within the laterally homogeneous and vertically stratified layered medium. The average structure is same as the structure presented in MODEL 1.

Table 2. Random structure (MODEL 2) for modelling L_g waves.

P Velocity km/s	S Velocity km/s	Density gm/cm^3	Thickness km	Q_β
5.4	3.103	2.78	1.0	250
5.7	3.276	2.84	1.0	250
5.5	3.161	2.8	1.0	250
6.0	3.448	2.9	1.0	250
5.8	3.333	2.86	1.0	250
6.26	3.620	2.952	3.0	250
6.45	3.670	2.99	8.0	500
6.5	3.736	3.0	1.6	500
6.4	3.678	2.98	1.6	500
6.6	3.793	3.02	1.6	500
6.5	3.736	3.0	1.6	500
6.7	3.851	3.04	1.6	500
6.8	3.908	3.06	1.571	500
6.6	3.793	3.02	1.571	500
7.2	4.138	3.14	0.858	2500
7.2	4.138	3.14	7.031	2500
6.8	3.908	3.06	1.571	2500
7.6	4.368	3.22	1.571	2500
7.2	4.138	3.14	1.571	2500
7.8	4.483	3.26	1.571	2500
8.1	4.6	3.32	10.0	2500
8.35	4.7	3.37	10.0	2500
8.4	4.755	3.38	10.0	2500
8.41	4.775	3.387	10.0	2500
8.42	4.794	3.393	10.0	2500
8.421	4.813	3.4	10.0	2500
8.422	4.833	3.407	10.0	2500
8.425	4.852	3.413	10.0	2500
8.43	4.871	3.42	10.0	2500

Herrmann 1987; Gupta *et al.* 1989). For this study, the Q model was as follows. The Q_β (shear-wave Q) for the upper 8 km of the crust was 250 and for the next 17.5 km was 500. The remaining crust has a Q_β of 6200. The Q_α (compressional-wave Q) was two times of Q_β in the upper crust of 25.5 km. For the remaining crust, Q_α was 8600. These Q values are comparable to the values cited in the above references.

Regional seismograms were synthesized at ECTN stations for three different source depths of 6, 10 and 28 km, using both elastic and anelastic crustal models (MODEL 1 and MODEL 2). The anelasticity was introduced by making the velocities complex (Kennett 1975). At each depth, these seismograms were used to investigate the effects of: (i) scattering (Q_s) caused by the velocity fluctuation, which was done by comparing the elastic results of MODEL 1 and MODEL 2; and (ii) anelasticity (Q_i), by comparing the results of the elastic and the anelastic calculations. These effects were then compared with the combined effect of velocity fluctuation and anelasticity together. In Fig. 12, we display 30 s of the P_{nl} seismograms from MODEL 1 and MODEL 2 at three depths and three distances (311, 391, and 616 km) for both elastic and anelastic cases. Each anelastic seismogram is plotted beneath each elastic seismogram. Both elastic and anelastic seismograms synthesized using MODEL 1 appear remarkably similar at all depths and distances except for the peak amplitudes; the same is true for MODEL 2 also. However, those synthesized using MODEL 2 display a significant increase in the strength of the various high-frequency phases relative to the phase with peak amplitude shown for MODEL 1, especially in the seismograms at 311 and 391 km. For example, the third largest distinct phase in amplitude (311 km for the source depth of 6 km) in MODEL 1, is not the largest in MODEL 2. Richards & Menke (1983) suggested that the effect of a crustal medium consisting of thin layers with alternate high and low velocities is to reduce the high-frequency aspects. This does not appear to be obvious in these simulated seismograms. The low-pass phenomenon discussed in Richards & Menke (1983) is possibly associated directly with the level of model discretization and distance. Fig. 13 displays synthetic L_g seismograms for the combinations of crustal structures, Q models and source depths. The L_g seismograms appear to be affected more than their counterpart S_{nl} waves by the crustal models and by the source depth. Clearly, the L_g waves have longer duration for shallow source depths.

6 DISCUSSION AND CONCLUSIONS

We have presented a method useful for simulating high-frequency regional seismograms using a two-step

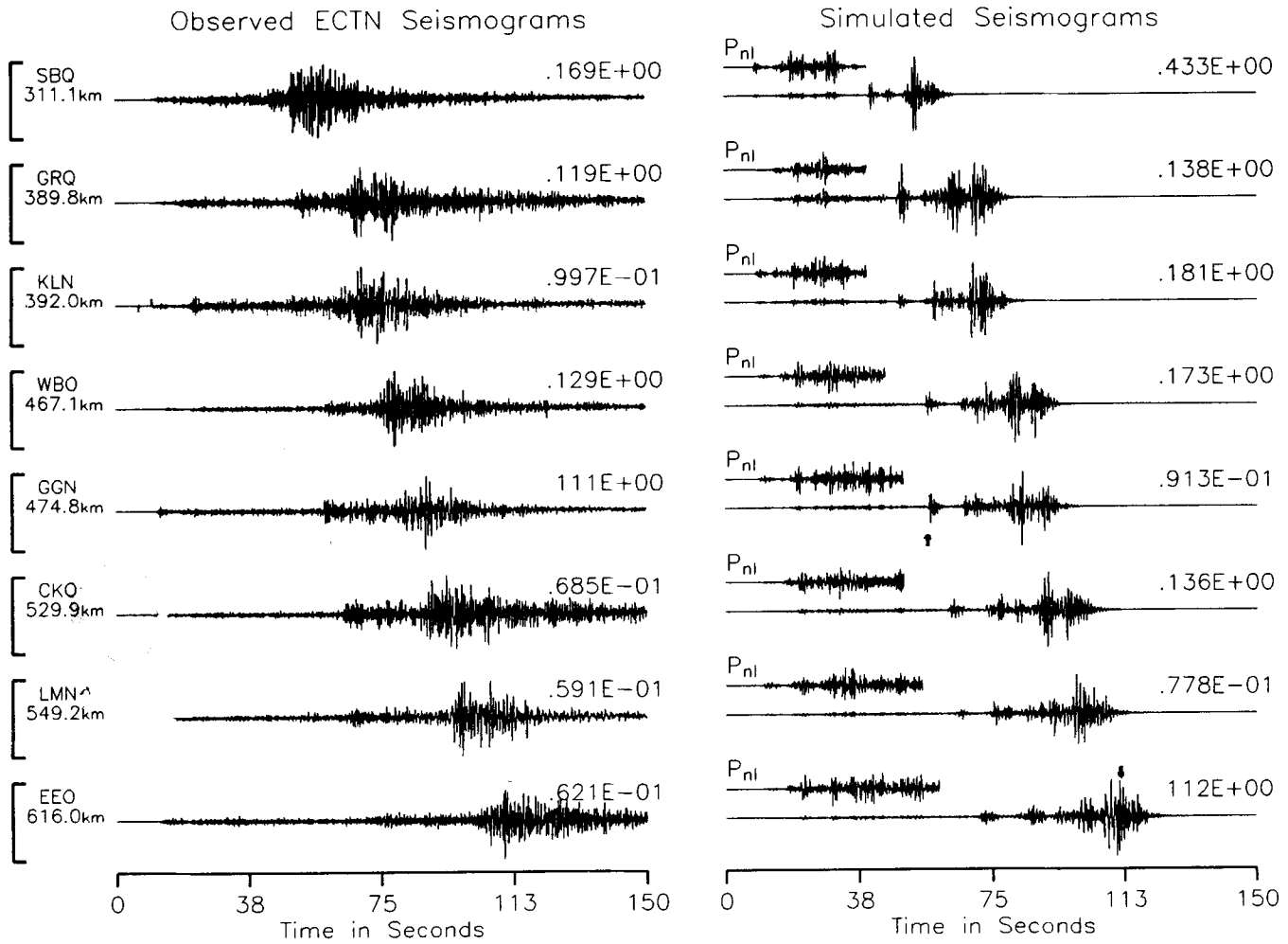

Figure 9. Comparison of the recorded ECTN seismograms with the synthetic seismograms computed using MODEL 2 shown in Fig. 8. The agreement in the L_g waves is much improved. The synthetic seismograms were computed using a seismic moment corresponding to a moment magnitude of 5.9. The peak amplitude of the simulated L_g waves agrees with the recorded peak L_g amplitude.

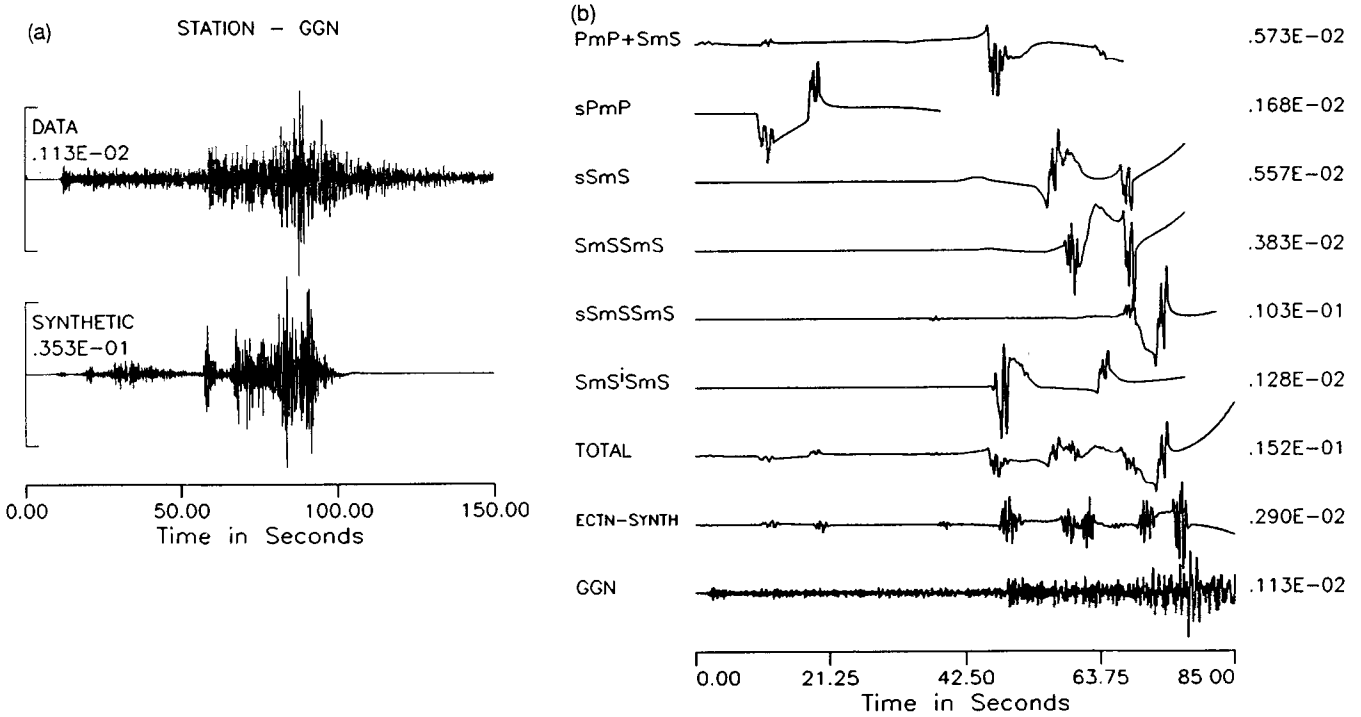

Figure 10. (a) Comparison between the data and synthetic seismogram computed for the ECTN instrument at GGN station. The station is located at a distance of about 475 km from the source. (b) Ray interpretation of the various phases that constitute the major phases recorded at station GGN.

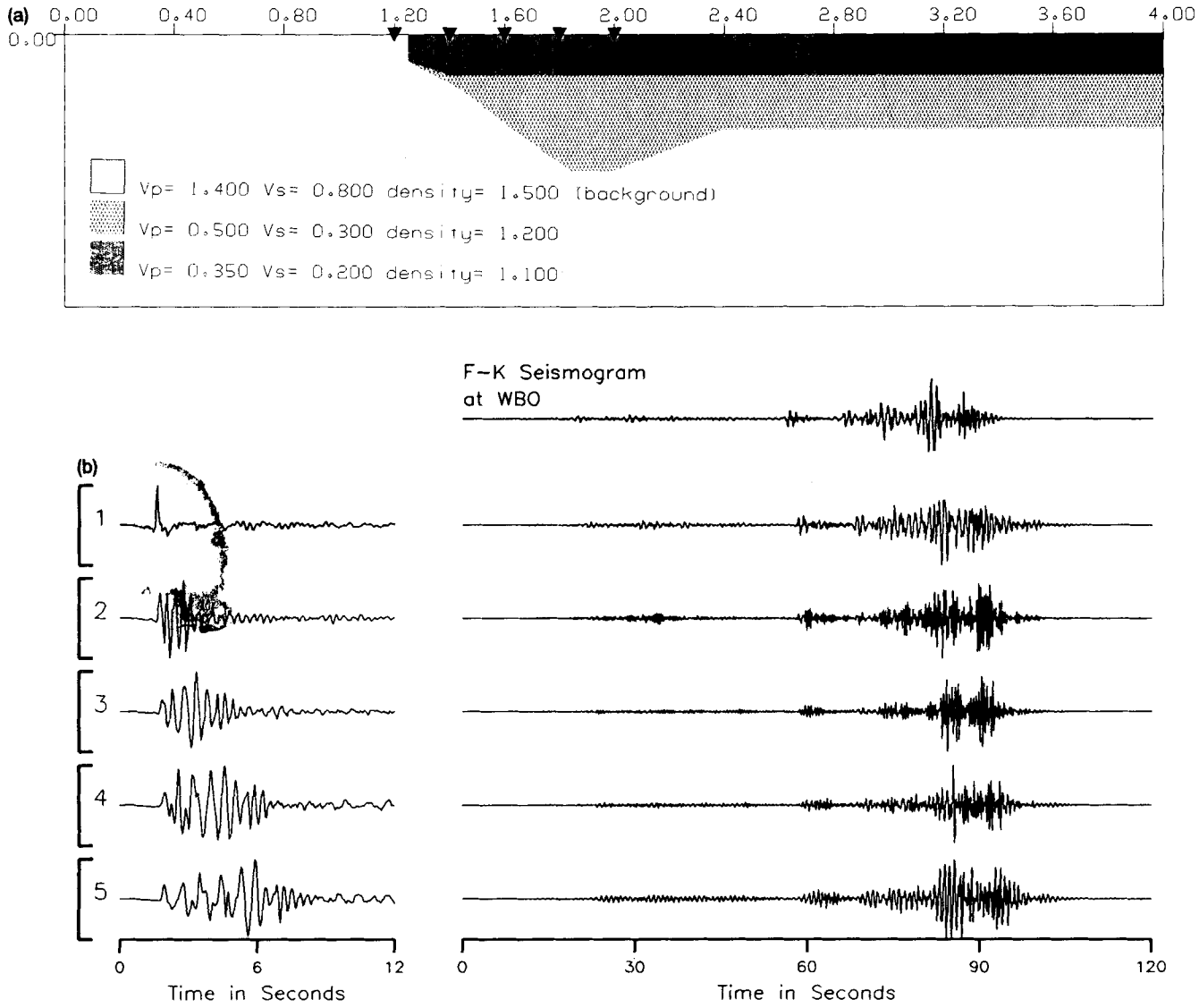

Figure 11. (a) A simplified 2-D crustal structure consisting of three layers designed to investigate its influence on the regional L_g seismograms. (b) The vertical *P–SV* seismograms (numbered 1 to 5) using an elastic finite-difference algorithm allowing *S* waves to impinge on the structure at an angle of 11°. The F-K seismogram at WBO is convolved with each seismogram shown on the left. The resulting seismogram is shown to its right. Although the duration in these seismograms has not changed, the frequency content of the seismograms is significantly affected.

procedure. In step one, the relative amplitudes and absolute traveltimes of various phases recorded on broad-band seismograms are used to calibrate an average crustal structure capable of modelling regional seismograms to a relatively high frequency. In step two, the waveguide is modified to simulate the early part of the most commonly observed high-frequency regional L_g waves by allowing seismic waves to propagate through a flat-layered laminated waveguide having alternate high and low velocities. This method has been validated by modelling regional L_g waves from the 1988 November 25 Saguenay earthquake recorded on the ECTN stations.

The source process of the Saguenay earthquake was complex. It is expected that such a complexity would influence regional seismograms. We have investigated the possible effects introduced by complex waveguides in a straightforward manner, using the published source information on the Saguenay event (Somerville *et al.* 1990; Zhao & Helmberger 1991; Haddon 1992). By successfully modelling the L_g waves from the Saguenay earthquake we have solved two major queries, one being related to the regional waveguide capable of trapping high-frequency L_g waves. We find that an average crustal model of the type shown in Fig. 5 fails to excite high-frequency L_g waves. There are several hypotheses on the physical mechanism of exciting these waves. The one that pertains to this study is a mechanism in which an alternate high- and low-velocity perturbation is used (e.g. O'Doherty & Anstey 1971; Richards & Menke 1983). As the alternating high- and low-velocity layering structure is introduced in the lower crust, the seismic paths corresponding to the various ray parameters leaving from the source change to different ray trajectories with different reflection and transmission coefficients across the interfaces. Consequently, the rays

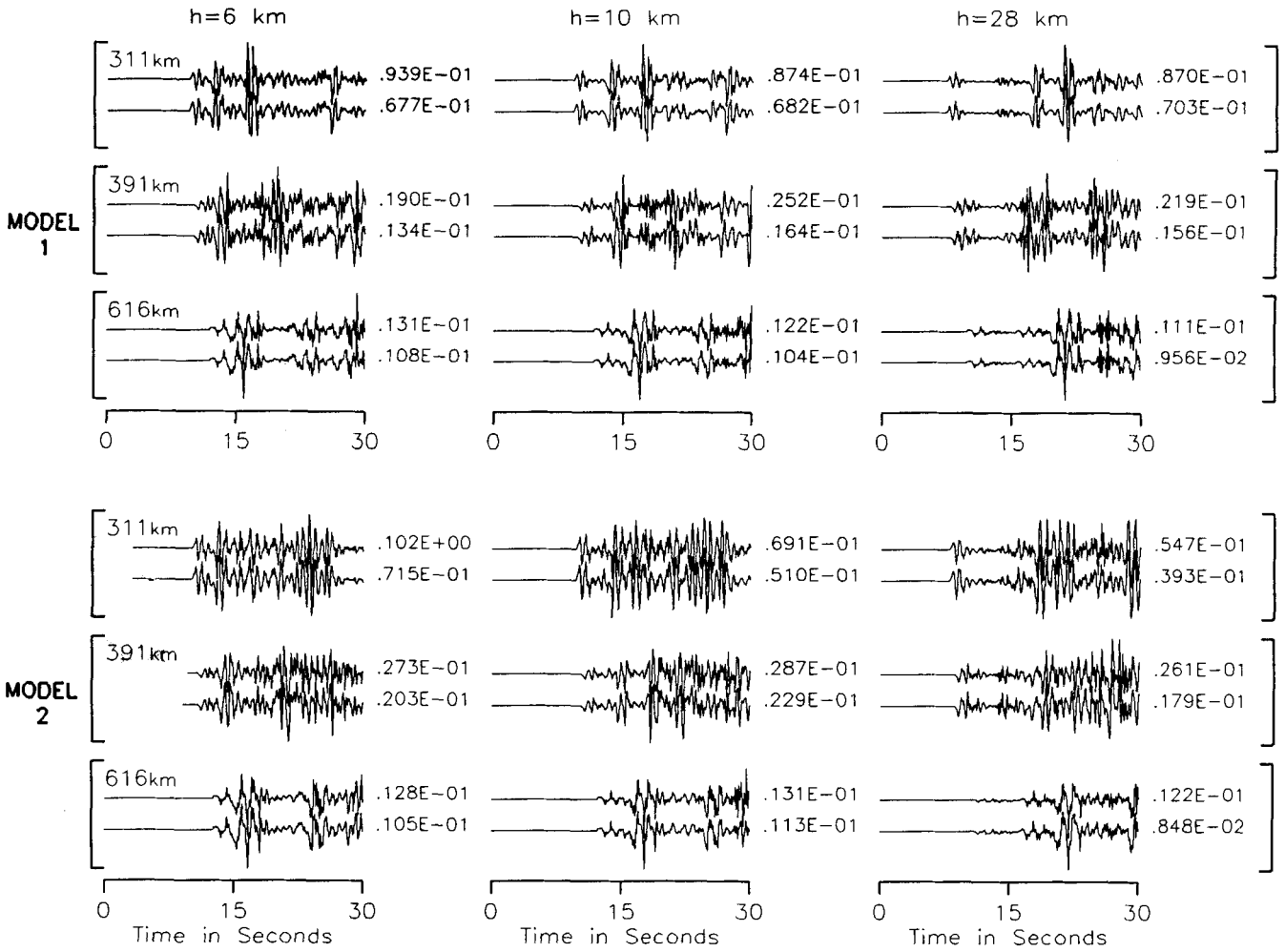

Figure 12. P_{nl} seismograms at three depths: 6, 10 and 28 km for both elastic and anelastic cases for crustal models MODEL 1 and MODEL 2. Each anelastic seismogram is shown below its equivalent elastic simulation.

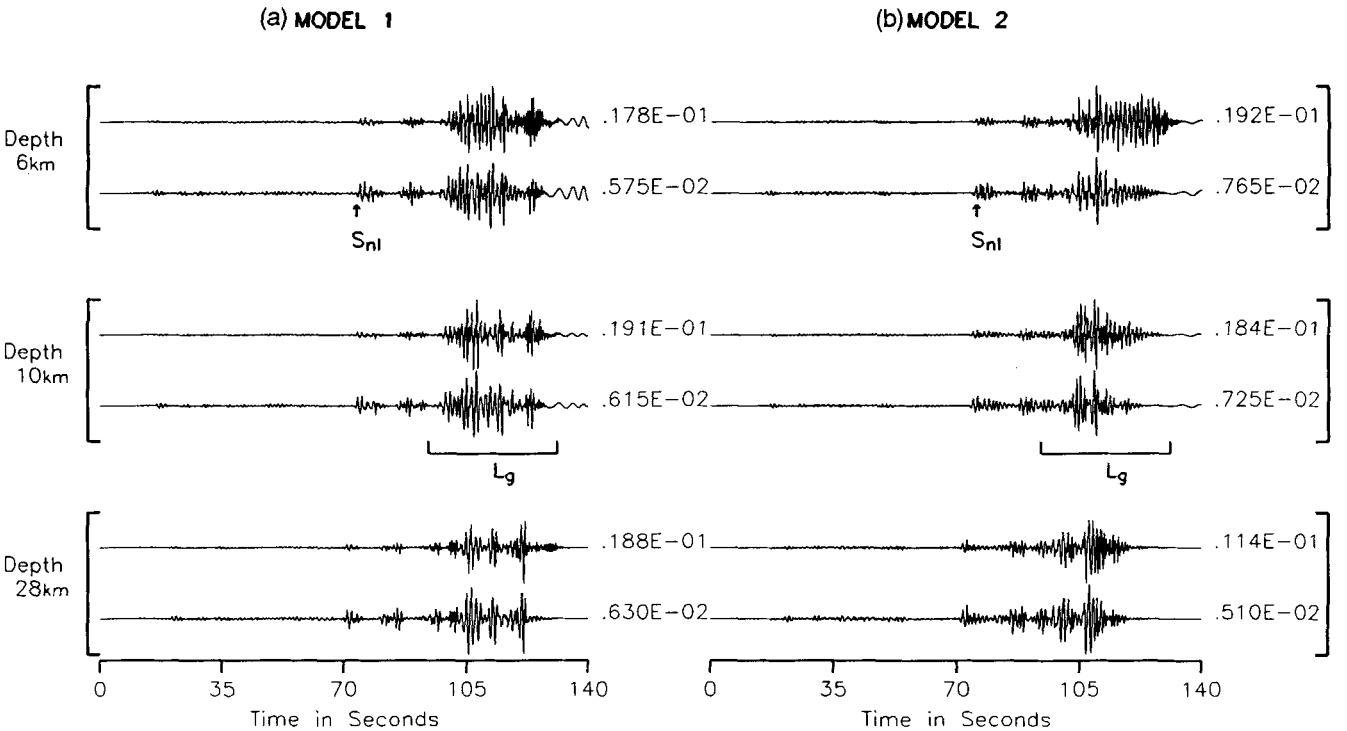

Figure 13. Schematic presentation of L_g waves at 616 km for three depths and two crustal models. (a) Crustal model is elastic; (b) crustal model is anelastic. Two seismograms are shown for each depth: the upper seismogram is computed using the elastic model and the lower seismogram is computed using the inelastic model.

arrive at a receiver with different traveltimes and amplitudes causing the rays to develop a constituent group of L_g waves.

The other enigma is related to its high m_{bLg} compared to its teleseismic m_b. We used a seismic moment consistent with the moment magnitude of 5.9 and predicted L_g peak amplitudes consistent with the observed peak values. Since the observations from the Saguenay earthquake are explainable on the basis of a wave propagation model coupled with the source depth, it is important that the experience gained from the Saguenay mainshock data is utilized in the prediction of future ground motions and earthquake-resistant design in eastern North America.

The recorded L_g seismograms could be modelled using a flat-layered structure. Other physical mechanisms are needed to account for the excitation of coda waves. One mechanism examined here allows the regional wavefield to interact with an irregular receiver structure. This mechanism is shown to have extended the duration of long-period surface waves (Campillo *et al.* 1988; Kawase & Aki 1989). The numerical results presented in this study show that such irregular receiver structures are also capable of trapping coda waves. The usefulness of such a concept is demonstrated through numerical experiments using a simplistic irregular receiver structure (Fig. 11). It was not the intention to model any data; it was rather to understand the influence of non-uniform structures on the wavefield. It may be worth pointing out that Barker *et al.* (1981) were also successful, to some degree, in simulating the amplification and envelope characteristics of L_g waves recorded at Yucca Flat using a similar 2-D calculation.

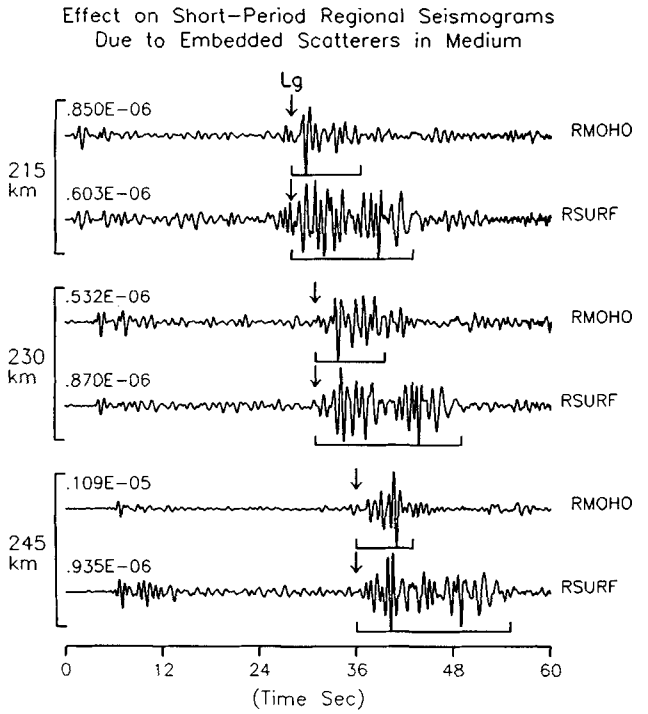

Figure 14. Simulated short-period seismograms (ECTN instrument response is added) using the medium response presented in Helmberger *et al.* (1993) for RMOHO and RSURF structures. For each pair, the lower seismogram (from the RSURF model) exhibits a distinctly longer duration for L_g coda (as marked by the arrow and the solid line) compared to the L_g waves excited in the RMOHO model (upper seismogram).

The presence of embedded scatterers in a medium also helps the excitation of L_g waves (Aki & Chouet 1975). Fig. 14 shows simulated regional ECTN seismograms using structures with scatterers randomly distributed in the thin layers at the top of the Moho discontinuity (RMOHO, upper seismogram) and in the layers near the surface (RSURF, lower seismogram; see Helmberger *et al.* 1993 for the model description). These wavefields were generated with a finite-difference scheme allowing velocity variation up to 20 per cent at each grid point (Frankel & Clayton 1984). This was done by permitting each grid point to have a random component with a Gaussian probability distribution. Actual finite-difference computation was performed using the technique discussed in Vidale & Helmberger (1987). As stated earlier, the S waves show a move-out with distance, energy being sustained noticeably over a longer duration, which may have developed by the backscattered waves from the scatterers present near the surface. In another study, Kennett & Mykkeltveit (1984) have interpreted the L_g waves observed in north-western Europe as the guided waves propagating through a laterally varying medium.

The final part of this paper included the results from several numerical simulations to explain the effect of Q_s and Q_l. Based on these simulations, we find that the L_g seismograms are affected more significantly by the nature of the waveguides and by the source depth than by their counterpart P_{nl} waves.

ACKNOWLEDGMENTS

The author is thankful to Professor D.V. Helmberger, at CIT, for his interest and comments in this study. I thank the Earth Physics branch, Ottawa, Canada for making the ECTN seismograms available to this study. I thank Steven N. Ward, an editor of GJI, and two anonymous reviewers for their useful comments which helped in improving the manuscript. Thanks to P.G. Somerville of Woodward-Clyde Consultants (WCC) for reviewing the manuscript. Special thanks to Robert W. Graves of WCC and Douglas Dreger of University of California at Berkeley who made the 2-D Green's functions available to me. This work was partially supported by Advanced Research Projects Agency under the contract F29601-91-C-DB01.

REFERENCES

Abramowitz, M. & Stegun, I.A., 1970. *Handbook of Mathematical Functions*, Dover Publications, New York.

Aki, K., 1969. Analysis of the seismic coda of local earthquakes as scattered waves, *J. geophys. Res.*, **74,** 615–631.

Aki, K. & Chouet, B., 1975. Origin of coda-waves: source, attenutation, and scattering effects, *J. geophys. Res.*, **80,** 3222–3342.

Aki, K. & Richards, P.G., 1980. *Quantitative Seismology—Theory and Methods*, Vol. 2, W.H. Freeman, New York.

Bard, P.-Y., Campillo, M., Chavez-Garcia, F.J. & Sanchez-Sesma, F., 1988. The Mexico earthquake of September 19, 1985—A theoretical investigation of large- and small-scale amplification effects in the Mexico City Valley, *Earthq. Spectra*, **4,** 609–633.

Barker, B.W., Der, Z.A. & Mrazek, C.F., 1981. The effect of crustal structure on the regional phases P_g and L_g at the Nevada test site, *J. geophys. Res.*, 1686–1700.

Boore, D.M. & Atkinson, G.M., 1992. Source spectra for the 1988 Saguenay, Quebec, earthquakes, *Bull. seism. Soc. Am.*, **82,** 683–719.

Bouchon, M., 1981. A simple method to calculate Green's functions for elastic layered media, *Bull. seism. Soc. Am.*, **71,** 959–971.

Campillo, M. & Paul, A., 1992. Influence of the lower crustal structure on the early coda of regional seismograms, *J. geophys. Res.*, **97,** 3405–3416.

Campillo, M., Bouchon, M. & Massinon, B., 1984. Theoretical study of excitation, spectral characteristics, and geometrical attenuation of regional seismic phases, *Bull. seism. Soc. Am.*, **74,** 79–90.

Campillo, M., Bard, P.Y., Nicollin, F. & Sanchez-Sesma, F., 1988. The Mexico earthquake of September 19, 1985—The incident wavefield in Mexico City during the great Michoacan earthquake and its interaction with deep basin, *Earthq. Spectra,* **4,** 591–608.

Dreger, D.S. & Helmberger, D.V., 1991. Complex faulting deduced from broadband modeling of the 28 February 1990 Upland earthquake, ($M_L = 5.2$), *Bull. seism. Soc. Am.*, **81,** 1129–1144

Dunkin, J.W., 965. Computation of modal solutions in layered, elastic media at high frequencies, *Bull. seism. Soc. Am.*, **55,** 335–358

Frankel, A. Clayton, R.W., 1984. A finite difference simulation of wave propagation in two-dimensional random media, *Bull. seism. Soc. Am.*, **74,** 2167–2186.

Frazer, L.N., 1977. Synthesis of shear-coupled PL, *PhD thesis,* Princeton University, Princeton, NJ.

Frazer, L.N. & Gettrust, J.F., 1984. On a generalization of Filon's method and the computation of the oscillatory integrals of seismology, *Geophys. J.R. astr. Soc.*, **76,** 461–481.

Fuchs, K. & Muller, G., 1971. Computation of synthetic seismograms with reflectivity method and comparison with observations, *Geophys. J. R. astr., Soc.*, **23,** 417–433.

Gupta, I.N., McLaughlin, K.L., Wagner, R.A., Jih, R.S. & McElfresh, T.W., 1989. *Seismic attenuation in eastern North America,* Rep. NP-6304, Research Project 2556-9, Electric Power Research Institute, Palo Alto, California.

Haddon, R., 1992. Waveform modeling of strong-motion data for the Saguenay earthquake of 25 November 1988, *Bull. seism. Soc. Am.*, **82,** 720–754.

Hasegawa, H.S., 1983. L_g spectra of local earthquakes recorded by the Eastern Canadian Telemetered network and spectral analysis, *Bull. seism. Soc. Am.*, **73,** 1041–1062.

Haskell, N.A., 1964. Radiation pattern of surface waves from point sources in a multilayered medium, *Bull. seism. Soc. Am.*, **54,** 377–393.

Helmberger, D.V., Dreger, D., Stead R. & Kanamori, H., 1993. Impact of broadband seismology on the understanding of strong motions, *Bull seism. Soc. Am.*, **83,** 830–850.

Herrmann, R.B. & Wang, C.Y., 1985. A comparison of synthetic seismograms, *Bull. seism. Soc. Am.*, **75,** 41–56.

Kawase, H. & Aki, K., 1989. A study of response of soft basin for incident *S, P,* and Rayleigh waves with special reference to long duration observed in Mexico City, *Bull. Seism. Soc. Am.*, **79,** 1361–1382.

Kennett, B.L.N., 1975. The effects of attenuation on seismograms, *Bull. seism. Soc. Am.*, **65,** 1643–1651.

Kennett, B.L.N., 1980. Seismic waves in a stratified half space—II. Theoretical seismograms, *Geophys. J.R. astr. Soc.*, **61,** 1–10.

Kennett, B.L.N. & Mykkeltveit, S., 1984. Guided wave propagation in laterally varying media—II. L_g waves in north-western Europe, *Geophys. J.R. astr. Soc.*, **79,** 257–267.

Kim, W.-Y., 1987. Modelling short-period crustal phases at regional distances for the seismic source parameter inversion, *Phys. Earth planet. Inter.*, **47,** 159–178.

Kind, R., 1979. Extensions of the reflectivity method, *J. Geophys.*, **45,** 373–380.

Luco, J.E. & Apsel, R.J., 1983. On Green's functions for a layered half-space, Part I., *Bull. seism. Soc. Am.*, **73,** 909–929.

Mallick, S. & Frazer, L.N., 1988. Rapid computation of multi-offset vertical seismic profile synthetic seismograms for layered media, *Geophysics,* **53,** 479–491.

Mallick, S. & Frazer, L.N., 1990. $P_o : S_o$ synthetics for a variety of oceanic models and their implications for the structure of the oceanic lithosphere, *Geophys. J. Int.*, **100,** 235–253.

North, R.G., Wetmiller, J., Adams, E., Anglin, F.M., Hasegawa, H.S., Lamontagne, M., Berger, R., Seeber, L. & Armruster, J., 1989. Preliminary results from the November 25, 1988 Saguenay (Quebec) earthquake, *Seism. Res. Lett.*, **60,** 89–93.

O'Doherty, R.F. & Anstey, N.A., 1971. Reflections on amplitudes, *Geophys. Prosp.*, **19,** 430–458.

Olsen, K.H., Braile, L.W. & Stewart, J.N., 1983. Modeling short-period crustal phases ($\bar{P}$, L_g) for long-range refraction profiles, *Phys. Earth planet. Inter.*, **31,** 334–347.

Richards, P.G. & Menke, W., 1983. The apparent attenuation of a scattering medium, *Bull. seism. Soc. Am.*, **73,** 1005–1021.

Saikia, C. K. & Burdick, L. J., 1991. Fine structure of P_{nl} waves from explosions, *J. geophys. Res.*, **96,** 14 383–14 401.

Saikia, C.K. & Helmberger, D.V., 1993. Broadband modeling of regional seismograms in Asia and the development of low-magnitude event discriminants, Final report to Phillips Laboratory, Contract no. FZ9G01-91-C-DB01, Kirkland Air Force Base, New Mexico.

Saikia, C.K., Helmberger, D.V. & Burdick, L.J., 1992. Regional wave propagation and high-frequency/low-frequency energy level discriminants, *14th Annual PL/DARPA Seis. Res. Symp.*, 16–18 September, Lowes Ventana Canyon Resort, Tucson, Arizona, pp. 351–360.

Saikia, C.K., Dreger, D.G. & Helmberger, D.V., 1994. Modeling of energy amplification recorded with Greater Los Angeles using irregular basin structure, *Bull. seism. Soc. Am.*, **84,** 47–61.

Shin, T.-C. & Herrmann, R.B., 1987. L_g attenuation and source studies using 1982 Miramichi data, *Bull. seism. Soc. Am.* **77,** 384–397.

Somerville, P.G., McLaren, J., Saikia, C. K. & Helmberger, D.V., 1990. The November 25, 1988 Saguenay Quebec earthquake: source parameters and the attenuation of strong ground motions, *Bull. seism. Soc. Am.*, **80,** 1118–1143.

Tolstoy, I. & Clay, C.S., 1966. *Ocean Acoustics,* McGraw-Hill, New York.

Vidale, J.E. & Helmberger, D.V., 1987. Seismic strong motion synthetics, in *Computational Techniques—4,* pp. 237–317, Academic Press, Orlando, Florida.

Vogfjord, K.S., & Langston, C.A., 1991. Analysis of regional events recorded at NORESS, *Bull. seism. Soc. Am.*, **80,** 2016–2031.

Wang, C.Y. & Herrmann, R.B., 1980. A numerical study of *P, SV* and *SH* wave generation in a plane layered medium, *Bull. seism. Soc. Am.*, **70,** 1015–1036.

Watson, T.H., 1970. A note on fast computation of Rayleigh wave dispersion in the multi-layered elastic half space, *Bull. seism. Soc. Am.*, **60,** 161–166.

Wu, R.S., 1985. Multiple scattering and energy transfer of seismic waves—separation of scattering effect from intrinsic attenuation—I. Theoretical modelling, *Geophys. J. R. astr. Soc.*, **82,** 57–80.

Zhao, L.S. & Helmberger, D.V., 1991. Broad-band modelling along a regional shield path, Harvard recording of the Saguenay earthquake, *Geophys. J. Int.*, **105,** 301–312.

APPENDIX

In this section, we only review the part of the derivation pertinent to demonstrate the computational efficiency of the frequency-wavenumber algorithm. In a medium consisting of n laterally homogeneous layers and source embedded at an interface m, the expressions for the F-K kernels can be shown to have the following forms

$$F(k, \omega) = \begin{pmatrix} U_r \\ U_z \end{pmatrix} = -\frac{1}{\mathbf{R}|_{12}^{12}} \begin{pmatrix} \zeta_i X|_{ij}^{12} Z_{j2} \\ -\zeta_i X|_{ij}^{12} Z_{j1} \end{pmatrix}, \tag{A1}$$

where the compound matrices $\mathbf{X}|_{12}^{ij}$ and $\mathbf{R}|_{12}^{12}$, derived using the product of matrices of subdeterminants, (Dunkin 1965) are given by

$$\begin{aligned} \mathbf{X}|_{ij}^{12} &= (FE_n^{-1})|_{mn}^{12} a_{n-1}|_{op}^{mn} \cdots a_{m+1}|_{ij}^{st} \\ \mathbf{R}|_{12}^{12} &= (FE_n^{-1})|_{mn}^{12} a_{n-1}|_{pq}^{mn} \cdots a_1|_{12}^{st} \\ \mathbf{a}|_{ij}^{lk} &= a_{il} a_{jk} - a_{ik} a_{jl} \end{aligned} \tag{A2}$$

$$\mathbf{Z} = \sum a_m a_{m-1} \cdots a_1$$

where the a_{ij} are the elements of the original matrix of Haskell (1964). The explicit forms of FE_n^{-1}, $\mathbf{a}|_{kl}^{ij}$, and ζ_i (the source coefficients) are given by Wang & Herrmann (1980).

Eqs (A1) and (A2) allow the propagation of the stress displacement vector from a half-space through a stack of layers. However, in the present forms the evaluation of $\mathbf{X}|_{12}^{ij}$ and $\mathbf{R}|_{12}^{12}$ would require many multiplications of 6×6 matrices to be performed. But, similar to the $\mathcal{J}$ matrix of Watson (1970), the compound matrix $\mathbf{a}|_{kl}^{ij}$ can be reduced from a 6×6 form to a 5×5 form by using similarity relations between the third and fourth components. These relations allow the elimination of the third column and row from the $\mathbf{a}|_{ij}^{mn}$ matrix replacing the fourth row by

$$[2a|_{12}^{24}, 2a|_{13}^{24}, 2a|_{23}^{24} - 1, 2a|_{24}^{24}, 2a|_{34}^{34}]^T. \tag{A3}$$

The dropped component is reconstructed finally by multiplying the old fourth component by a correct scalar. However, to evaluate the medium response at the free surface by expression (A1), we need the elements of the first column of the $\mathbf{R}|_{ij}^{mn}$ and $\mathbf{X}|_{ij}^{mn}$ matrices. This means we do not need to perform the multiplications even of the 5×5 matrices for propagating the stress-displacement vectors through the stack of layers. Instead, we require a multiplication of a 5×5 matrix with a 5×1 matrix. Together with the Filon's quadrature, this makes the wave propagation through the medium computationally fast, especially at high frequencies.